Supplementary Materials for

Bioinspired handheld time-share driven robot with expandable dexterity

Yunjiang Wang *et al.*

Corresponding author: Haoran Jin, jinhr@zju.edu.cn

The PDF file includes:

Other Supplementary Material for this manuscript includes the following:

Movie S1. Demonstration of the SMA clutch response to PWM input.

Movie S2. Demonstration of the bending motion of one bending module.

Movie S3. Demonstration of two bending modules working cooperatively.

Movie S4. Demonstration of modular assembly of time-share driven robot.

Movie S5. Demonstration of diagnosis experiment in human stomach model.

Movie S6. Demonstration of therapy experiment in ex vivo porcine stomach.

1. Comparison of this work with continuum robot designs.

The comparison of main continuum robot designs is listed in Table. S1. Limited by the manufacturing process, it is prohibitive to build more than two segments in tendon-driven and multi-backbone designs, and more than three segments in concentric tube design. Good maneuverability for their designs, though, the DoFs are limited to six to keep a satisfying footprint for surgery application. This work adopted one segment of multi-backbone designs and connected a variable number of BMs based on time-share driven mechanism. Benefiting from this mechanism, it is feasible to expand numbers of segments, while the cross-section of the manipulator keeps the same.

Tables S1. Comparison of this work with continuum robot designs

Continuum Designs for surgery	Controllable DoFs (Potential to be more than six)	Light-weight (Hand-held)	Task-oriented reconfiguration in situ	Model and control
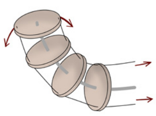 Tendon driven (*15,16,21*)	★★★☆☆ (1~2) $DoFs/seg$ × (1~3) seg	★★★☆☆ For manual control instruments	★☆☆☆☆ Tendons cannot be settled in situ	★★★☆☆ Close to constant curvature
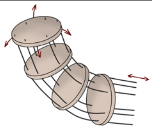 Multi-backbone (*17,22*)	★★★☆☆ (2~3) $DoFs/seg$ × (1~2) seg	★☆☆☆☆ Large and heavy motor package	★☆☆☆☆ Tendons cannot be settled in situ	★★★★☆ Fit well with constant curvature
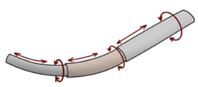 Concentric tube (*13*)	★★★☆☆ 2 $DoFs/seg$ × (2~3) seg	★★★★☆ Simple transmission structure	★★★☆☆ Simple assembly	★★☆☆☆ complicated by torsional deformation
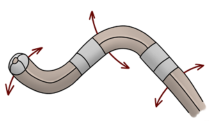 Soft robot (*20*)	★★★★★ (1~3) $DoFs/seg$ × n seg	★☆☆☆☆ Air/water pumps are heavy and noisy	★★★★☆ Modular assembled	★☆☆☆☆ complex connection between actuation and robot deformation
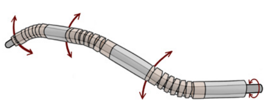 This work	★★★★☆ 1 DoF/seg × n seg	★★★★★ Motor base is 202 g	★★★★★ Multiple assembly configurations	★★★★★ decoupled BMs each BM fits constant curvature

DoF: Degree of freedom. Seg: Motion segment

2. Design process for key parameters of laser-profiled tubes

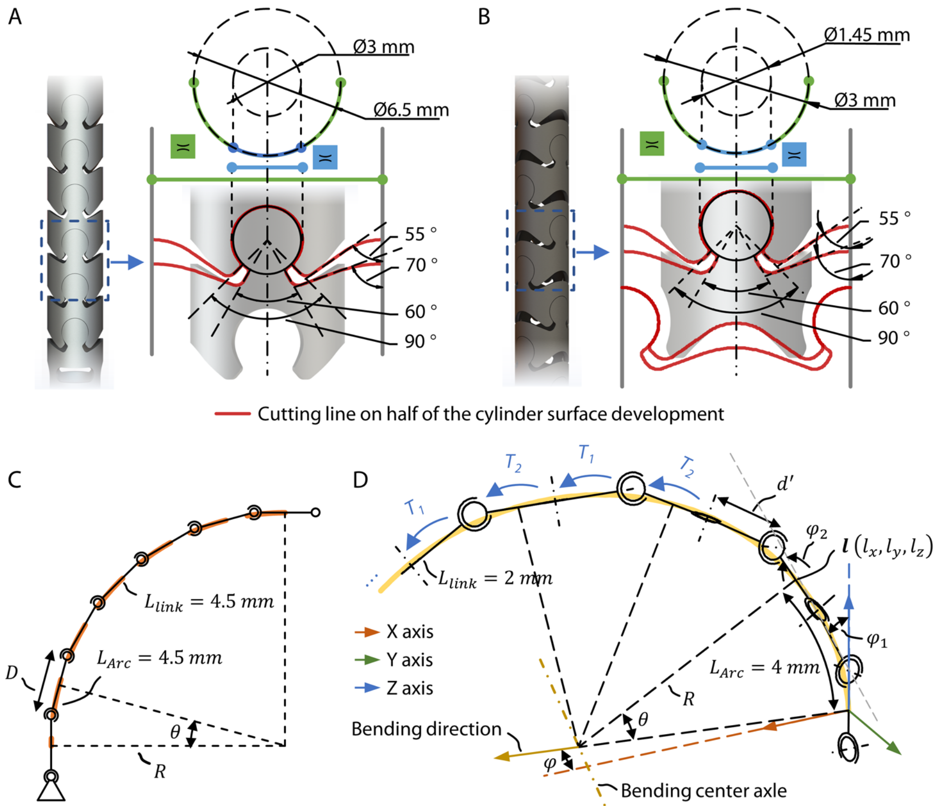

Fig. S1. Details of laser-profiled discrete-jointed tubes. (**A**) The key parameters of the discrete-jointed tube for PSS. (**B**) The key parameters of the discrete-jointed tube for FIS. (**C**) The kinematic model of the PSS tube. (**D**) The kinematic model of the FIS tube.

To cut a rotation joint on a stainless tube, the laser-profiled process on the cylindrical surface should divide the tube into a part with a circular arc notch locking the other part with a lug (Fig. S1A and B). The neck of the lug had an open angle of 60 deg, while the notch had an open angle of 90 deg, leaving a 30 deg elbow room for rotation on each side. This kind of laser-profiled tube, usually called serpentine tube, consists of a series of rotation joints and shows high stiffness for directions out-of-plane forces. The calculation of kinematics is complicated due to the large number of discrete joints. To address this, we simplified the bending motion as a constant-curvature deflection and proposed the joint shift correction method to validate the simplification in our design parameters. The main design parameters are listed in Table. S2.

For the PSS tube, to wear the bent discrete-jointed tube on a continuum tube, the middle part of each segment should fit on the arc line, as they were constrained more. Then all the adjacent segments were pulled apart because the length of the polyline is greater than the arc length of inscribed circle. The joint shift described the needed adjustment.

Tables S2. Parameters of the laser-profiled discrete-jointed tubes

	Parameter	Values
Plane bending tube	Link length of one segment (mm)	4.5
	Outer diameter (mm)	6.5
	The thickness of the tube (mm)	0.25
Printing parameters	Link length of one segment (mm)	2.0
	Outer diameter (mm)	3.0
	The thickness of the tube (mm)	0.2

In Fig. S1C, the arc between two segments is equal to L_{link}, which must satisfy

$$L_{link} = \theta \cdot R \tag{S1}$$

The new distance of the two adjacent joints should satisfy

$$D/2 = R \cdot \tan(\theta/2) \tag{S2}$$

Thus,

$$D = 2\tan(\theta/2) * L_{link}/\theta \tag{S3}$$

The clearance created by laser-profile technology is 30 μm, so we got the necessary condition

$$L_{joint\_shift} = D - L_{link} = (2\tan(\theta/2) - \theta) * L_{link}/\theta \leq 30\mu m \tag{S4}$$

According to Fig. 2B and Table S2, our design parameters satisfied Eq. S4. Using Eq. S1, the minimum bending radius 17.2 mm could be approached.

As for the FIS tube, the one-direction bending can be established by a combination of two orthometric rotations. It is implemented by two steps. Firstly, the rotation combination must produce a pure rotation. Secondly, the joint shift can be covered by a laser-profile gap so as for the discrete-jointed tube to fit a constant curve arc. The middle point of each segment is put on the arc for the same consideration as the PSS tube.

In Fig. S1D, we place the coordinate on the center of a link, which represents a segment of the tube. The next link rotates along the X-axis for an angle of φ_1, The next link rotates along the Y-axis of the former link for an angle of φ_2.

Follow the D-H method for modeling, considering the adjacent joint's distance d', we have the transfer matrix of the first rotation as

$$T_1 = \begin{bmatrix} 1 & 0 & 0 & 0 \\ 0 & cos(\varphi_1) & -sin(\varphi_1) & -d'sin(\varphi_1) \\ 0 & sin(\varphi_1) & cos(\varphi_1) & d'cos(\varphi_1) \\ 0 & 0 & 0 & 1 \end{bmatrix} \tag{S5}$$

and the second rotation as

$$T_2 = \begin{bmatrix} cos(\varphi_2) & 0 & sin(\varphi_2) & d'sin(\varphi_2) \\ 0 & 1 & 0 & 0 \\ -sin(\varphi_2) & 0 & cos(\varphi_2) & d'cos(\varphi_2) \\ 0 & 0 & 0 & 1 \end{bmatrix} \tag{S6}$$

The rotation combination can be calculated as the transfer matrix

$$T = T_1 * T_2 = \begin{bmatrix} c_2 & 0 & s_2 & d's_2 \\ s_1 s_2 & c_1 & -s_1 c_2 & -d's_1(1+c_2) \\ -c_1 s_2 & s_1 & c_1 c_2 & d'c_1(1+c_2) \\ 0 & 0 & 0 & 1 \end{bmatrix} \tag{S7}$$

where $sin(\varphi_k)$ are written as s_k for short, and $cos(\varphi_k)$ are written as $c_k, k = 1,2$.

The rotation matrix in Eq. S7 can be transferred to a representation of the angle axis as

$$R = [\theta \quad \boldsymbol{r}] = \begin{bmatrix} acos\left(\frac{c_1 + c_2 + c_1 c_2 - 1}{2}\right) & \frac{1}{2sin(\theta)} \begin{bmatrix} s_1(1+c_2) \\ s_2(1+c_1) \\ s_1 s_2 \end{bmatrix} \end{bmatrix} \tag{S8}$$

The translation vector $\boldsymbol{t}$ can be separated from the last column of Eq. S7 as

$$\boldsymbol{t} = \begin{bmatrix} d's_2 \\ -d's_1(1+c_2) \\ d'c_1(1+c_2) \end{bmatrix} \tag{S9}$$

It is clear that $\boldsymbol{t} \cdot \boldsymbol{r} \equiv 0$, so the three-dimensional motion is a pure rotation along an axle parallel to $\boldsymbol{r}$.

The distance between the two ends of an arc segment can be calculated by coordinates

$$\boldsymbol{l} = norm\left(\begin{bmatrix} d's_2/2 \\ -d's_1(1+c_2/2) \\ d'c_1(1+c_2/2) \end{bmatrix} + \begin{bmatrix} 0 \\ 0 \\ d'/2 \end{bmatrix}\right) \tag{S10}$$

According to *the Sines Law*, the bending radius R can be solved by

$$2R \cdot \sin(\theta/2) = d' \cdot norm\left(\begin{bmatrix} s_2/2 \\ -s_1(1+c_2/2) \\ c_1(1+c_2/2) \end{bmatrix} + \begin{bmatrix} 0 \\ 0 \\ 1/2 \end{bmatrix}\right) \tag{S11}$$

The curve length of the arc segment is a constant equaling $2L_{link}$, we have

$$R \cdot \theta = 2L_{link} \tag{S12}$$

Juggle the equations S11 and S12, eliminate R, we have

$$d' = L_{link} \cdot \left(\frac{4\sin(\theta/2)}{\theta}\right) / norm\left(\begin{bmatrix} s_2/2 \\ -s_1(1+c_2/2) \\ c_1(1+c_2/2)+1/2 \end{bmatrix}\right) \tag{S13}$$

For flexible bending, the joint shift can be calculated as

$$d' - L_{link} = \left(\frac{\left(\frac{4\sin\left(\frac{\theta}{2}\right)}{\theta}\right)}{norm\left(\begin{bmatrix} \frac{s_2}{2} \\ -s_1\left(1+\frac{c_2}{2}\right) \\ c_1\left(1+\frac{c_2}{2}\right)+\frac{1}{2} \end{bmatrix}\right)} - 1\right) \cdot L_{link} \leq 30\mu m \tag{S14}$$

where, θ can be solved in S8. According to Fig. 2D and Table S2. Our design parameters satisfied Eq. S14. The minimum bending radius could be calculated according to Eq. S12, which was around 15.3 mm. The maximum value of θ was set to 15 deg, which could be achieved at any bending direction (Fig. 2E).

Collectively, the bending of the laser-profiled discrete-jointed tube can be treated as a constant-curvature bending.

3. Details of the SMA wire testing platform

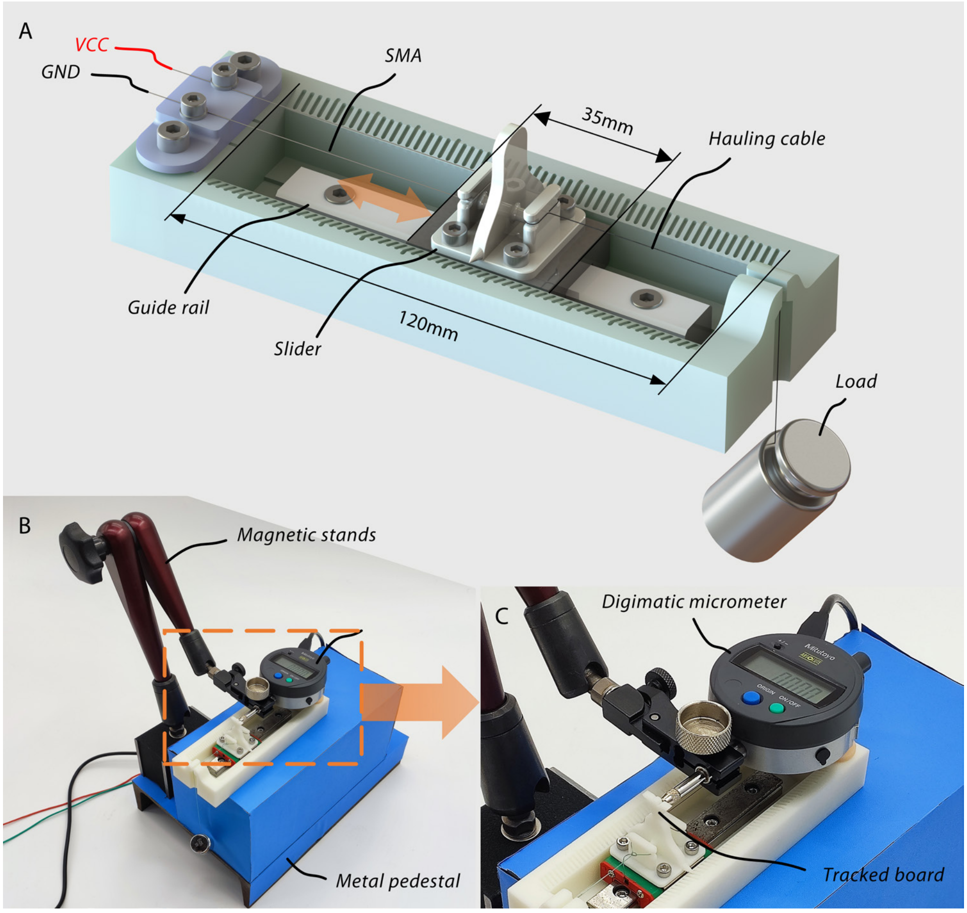

Fig. S2. Details of the SMA wire testing platform. (**A**) The model of the SMA wire testing platform. The slider was pulled by the SMA wire and a load on two ends. The friction was ignored. (**B**) The scene of the SMA wire testing. The resistance of the digimatic micrometer was considered a constant and added to the load. (**C**) The details of the tracked board. The motion of the slider was recorded by the digimatic micrometer.

4. Design of ETS

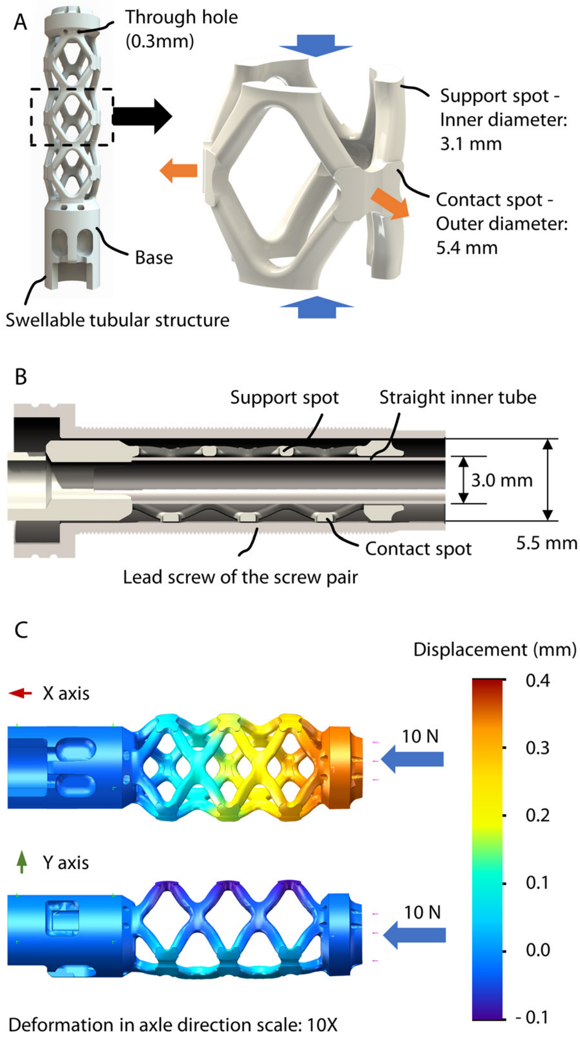

Fig. S3. Design of ETS. (**A**) Swellable element. An ETS contained three swellable elements. Each element consisted of six legs associated with three support spots on two ends. The knees of the legs folded on three contact spots. The compression on the support spots plane caused the knees to get pushed out. (**B**) The ETS worked as a clutch. The contraction of the ETS activated all of the contact spots to stick on the inner wall of the lead screw. All of the legs got support from the straight inner tube on the support spots. (**C**) The displacement of the ETS under 10 N force. The max axial displacement along the tube was around 0.3mm, and the radial displacement was around 0.1 mm, which was smaller than the distance between the contact spot and the inner wall of the lead screw (0.05 mm).

The design parameters of the ETS were concluded from the result of several rounds of testing and optimizations. The material was rigid resin. Its related parameters were listed in Table. S3. The statics analysis showed a 10 N force along the tube was enough to build a connection between the ETS and the lead screw of the screw pair.

Tables S3. Parameters of the rigid resin and 3D-print process

	Parameter	Values
Rigid resin	Hardness (D)	82
	Tensile Strength (MPa)	38
	Ultimate Elongation (%)	8
	Tensile Modulus (MPa)	1149
	Bending Strength (MPa)	49
	Flexural Modulus (MPa)	1476
Printing parameters	Nominal Resolution (μm)	35
	Slice Thickness (mm)	0.03
	Exposure time per layer (s)	1.2

5. The manufacturing process of the SMA clutch

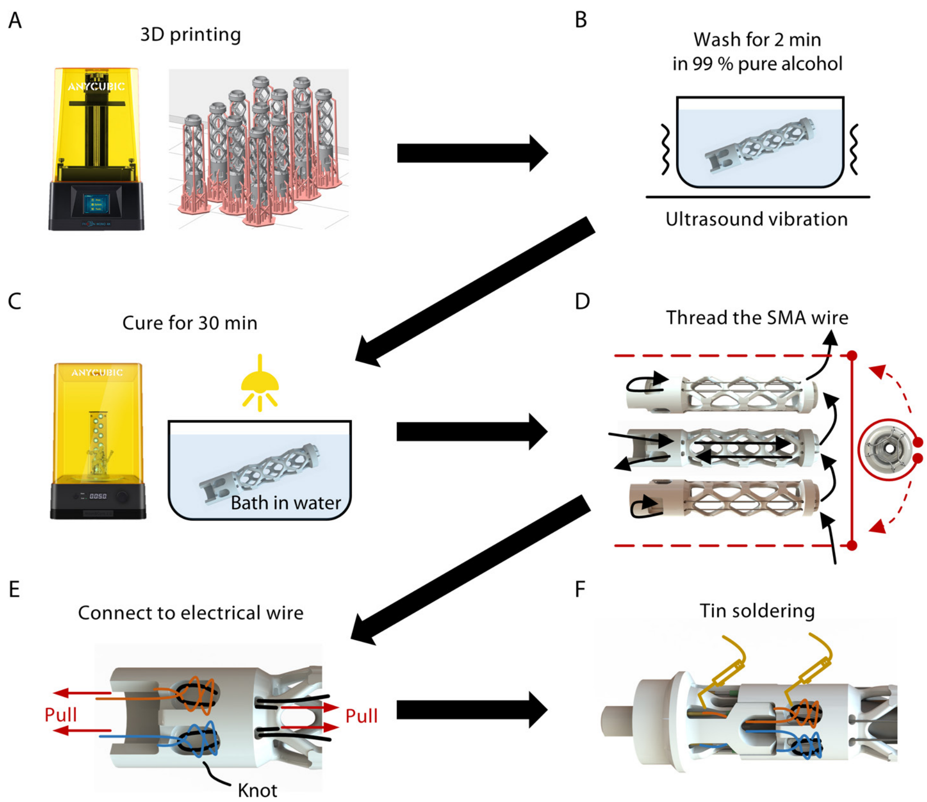

Fig. S4. The manufacturing process of the SMA clutch. (**A**) 3D-printing process. (**B**) Ultrasound cleaning. (**C**) Ultraviolet Curing. (**D**) Thread with the SMA wire. (**E**) Wiring. (**F**) Tin soldering.

The ETS was made by Laser cladding deposition 3D-printing. The model was bathed in 99% pure alcohol to wash the remaining liquid resin, especially in the through holes. The curing process was adopted to promote the final mechanical performance, and bathing in pure water helped to build a smooth surface. An SMA wire was threaded on the tube six times, circularly distributed. Tin is not adhesive to the SMA, so the welding spot may fall off and lose conductivity after several contractions. A feasible way was making a hard knot in the two pits of the swellable tubular structure, which provided room for tin soldering later. The temperature accumulation in soldering should be avoided. Both the rigid resin and the SMA wire could not bare temperatures over 200 °C for more than 10 s. A welding gun with temperature control was preferred. The temperature could be set to 240 °C, which is a little higher than the melting point of tin (231.93 °C).

6. The Fabrication process of one BM

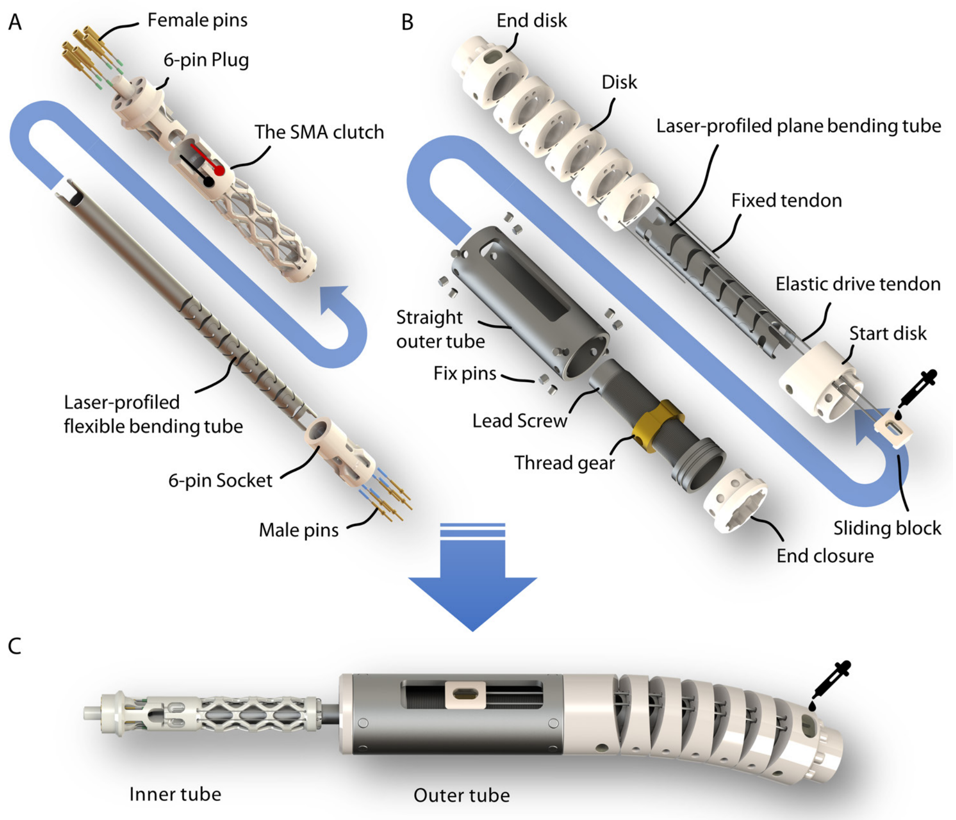

Fig. S5. The Fabrication process of one BM. (**A**) The fabrication process of FIS. The FIS contains the 6-pin Plug, the SMA clutch, the laser-profiled discrete-jointed tube, and the 6-pin socket, serially connected. The laser-profiled discrete-jointed tube has notches on two ends, to be plugged into the SMA clutch and the 6-pin socket, transmitting rotation. (**B**) The fabrication process of PSS. The bending part contains five disks. These disks were slipped into the laser-profiled discrete-jointed tube. Two fixed tendons went through the corresponding holes of disks. These disks were fixed on the fixed tendons by UV curable adhesive. The laser-profiled discrete-jointed tube was sealed by the start disk and the end disk. Two elastic drive tendons went through all the disks. One end of these tendons was fixed on the end disk, and the other end was fixed on the sliding block. The bending part was fixed on one end of the straight outer tube with the fixed pins. A screw pair was placed inside the tube. Then the tube was sealed with the end closure. (**C**) One BM. The FIS could be placed inside the PSS, then the whole BM was finished.

7. Modeling of the BM.

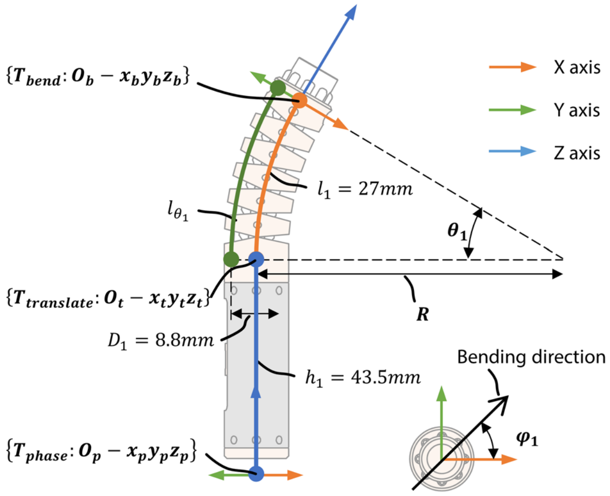

Fig. S6. Modeling of the BM. This module was fixed on the base or the former module with a phase (8 phases evenly distributed with a 45 deg interval). This module provided a fixed translation and a bending motion.

The PSS was designed to be bent to 90 deg on both sides. The modeling of one PSS includes three transfer matrices (Fig. S6).

The first is a rotation according to the installation phase of this segment

$$T_{phase} = \begin{bmatrix} cos\varphi_1 & -sin\varphi_1 & 0 & 0 \\ sin\varphi_1 & cos\varphi_1 & 0 & 0 \\ 0 & 0 & 1 & 0 \\ 0 & 0 & 0 & 1 \end{bmatrix} \tag{S15}$$

The second is a translation along the straight outer tube

$$T_{translate} = \begin{bmatrix} 1 & 0 & 0 & 0 \\ 0 & 1 & 0 & 0 \\ 0 & 0 & 1 & h_1 \\ 0 & 0 & 0 & 1 \end{bmatrix} \tag{S16}$$

where the h_1 represents the length of the rigid part.

The third is the bending motion

$$T_{bend} = \begin{bmatrix} \cos\theta_1 & 0 & \sin\theta_1 & l_1 \cdot (1 - \cos\theta_1)/\theta_1 \\ 0 & 1 & 0 & 0 \\ -\sin\theta_1 & 0 & \cos\theta_1 & l_1 \cdot \sin\theta_1 /\theta_1 \\ 0 & 0 & 0 & 1 \end{bmatrix} \tag{S17}$$

where, the l_1 represents the length of the bending part.

The transfer matrix of this bending module can be solved using the chain rule

$$T_{bm\,1} = T_{phase} \cdot T_{translate} \cdot T_{bend}$$
$$= \begin{bmatrix} cos\varphi_1 \cos\theta_1 & -sin\varphi_1 & cos\varphi_1 \sin\theta_1 & l_1 cos\varphi_1 \cdot \dfrac{(1-\cos\theta_1)}{\theta_1} \\ sin\varphi_1 \cos\theta_1 & cos\varphi_1 & sin\varphi_1 \sin\theta_1 & l_1 sin\varphi_1 \cdot \dfrac{(1-\cos\theta_1)}{\theta_1} \\ -\sin\theta_1 & 0 & \cos\theta_1 & l_1 \cdot \dfrac{\sin\theta_1}{\theta_1} + h_1 \\ 0 & 0 & 0 & 1 \end{bmatrix} \tag{S18}$$

where θ_1 is a function of l_{θ_1}, which represents the curve length of the driven cable in the bending part. In Fig. S6C, we have

$$R \cdot \theta_1 = l_1 \tag{S19}$$

and

$$(R + D_1/2) \cdot \theta_1 = l_{\theta_1} \tag{S20}$$

Minus Eq. S20 with Eq. S19, we got

$$\theta_1 = 2\left(l_{\theta_1} - l_1\right)/D_1 \tag{S21}$$

The kinematic model of one PSS can be represented by Eq. S18, and θ_1 can be determined by Eq. S21. Other constants are marked in Fig. S6C.

8. The Fabrication process of the time-share driven robot

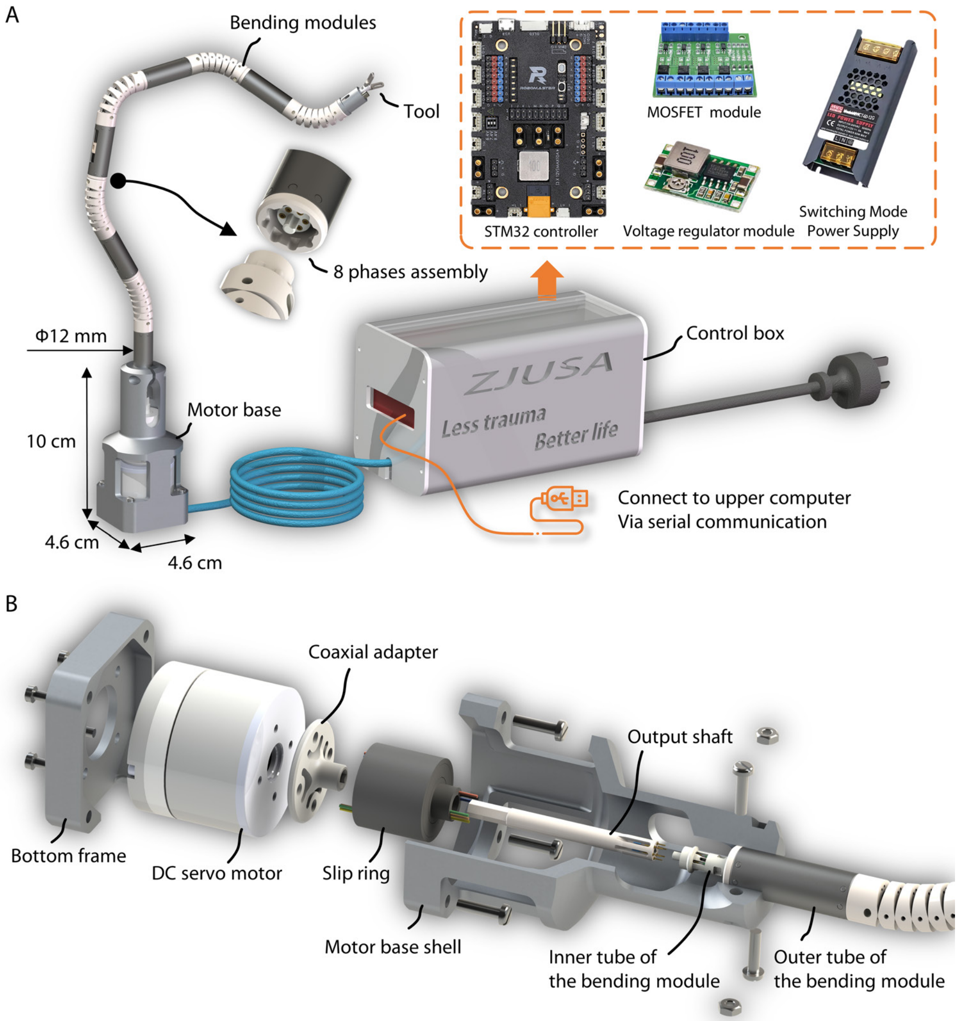

Fig. S7. The Fabrication process of the time-share driven robot. (**A**) The rendering of the time-share driven robot. The base BM was fixed on the motor base. The next BM was fixed on the former bending module with an eight phases assembly. The tool was fixed on the last BM. The wires required by other tools go outside along the manipulator. The motor base was connected to a control box. Inside the control box, the STM32 controller board was powered by the Switching Mode Power Supply with a 24 V input. The power supply to SMA clutches was from the Voltage regulator module with a 5 V output. This was controlled by the multi-channel MOSFET module with multi-channel PWM input from the STM32 controller. (**B**) The explosion view of the motor base.

9. Modeling and the analysis of the time-share driven robot

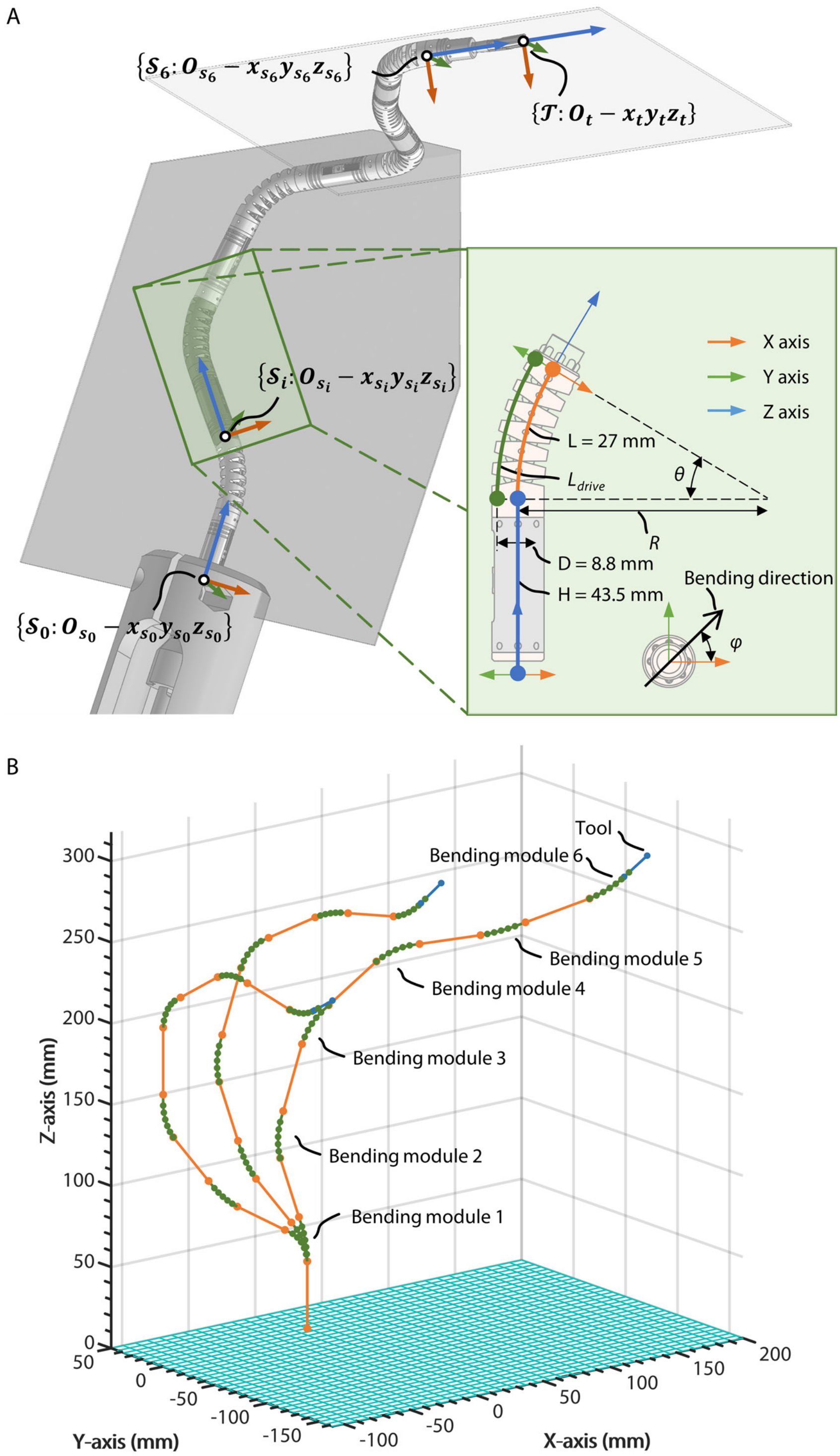

Fig. S8. Modeling and the analysis of the time-share driven robot. (**A**) The modeling of the time-share driven robot consisted of six BMs. (**B**) The kinematic model.

Considering the number of BMs and the assemble combination phases, the model of the time-share driven robot is determined by an installation vector $\boldsymbol{\varphi} = [\varphi_1 \quad \varphi_2 \quad \cdots \quad \varphi_n]$ and the design parameters of each BM. If not considering the extension tube, according to Eq. S18, the tip position of the time-share driven robot can be represented in Eq. S22

$$T_{robot} = T_{bm\,1}(l_1, \quad h_1, \quad \varphi_1, \quad \theta_1) * \cdots * T_{bm\,n}(l_n, \quad h_n, \quad \varphi_n, \quad \theta_n) * T_{tool} \quad \text{(S22)}$$

Once the installation vector is settled, the tip position is only determined by $\boldsymbol{\theta}$

$$T_{robot} = T_{bm\,1\sim n}(\theta_1 \quad \theta_2 \quad \cdots \quad \theta_n) * T_{tool}$$
$$\theta_i = 2(p \cdot r_i - l_i)/D_i \quad \text{(S23)}$$

where, according to Eq. S21, p is the lead of the lead screw. Here, the lead is equal to the helical pitch – 0.25 mm. r_i is the number of turns of each screw pair.

10.Demonstration of diagnosis experiment in a human stomach model

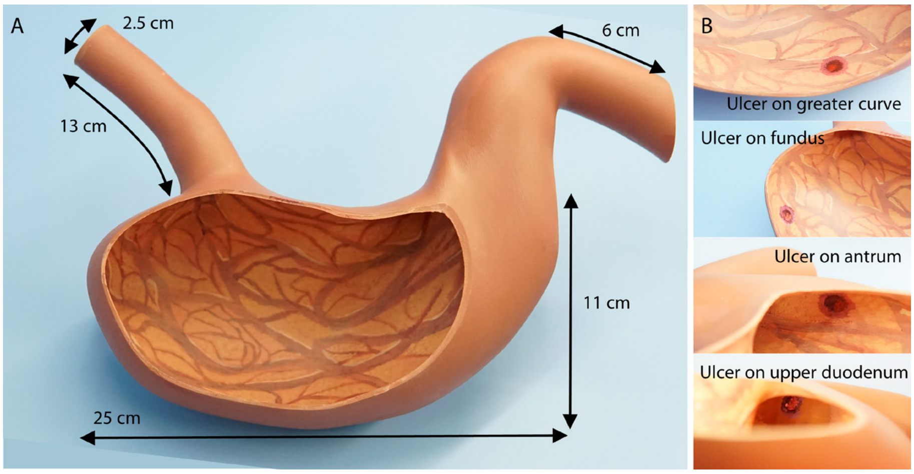

Fig. S9. Demonstration of diagnosis experiment in a human stomach model. (**A**) The human stomach model used in the diagnostic experiment was 3D printed. The stomach model was 25 cm in length and 11cm in width. The continuous esophagus was 13 cm long and the inner diameter was 2.5 cm. The continuous upper part of the duodenum was 6 cm. The outer surface of the model was painted to simulate the stomach, vessels and mucosa were drawn on the inner surface of the model to simulate the morphology of gastric mucosa. These were helpful to tip positioning or guide the motion direction in endoscopic view by the operator. (**B**) Ulcers were drawn on the inner wall of the stomach model at four anatomical locations as lesions in diagnosis experiments.

11.Demonstration of therapy experiment in an excised porcine stomach

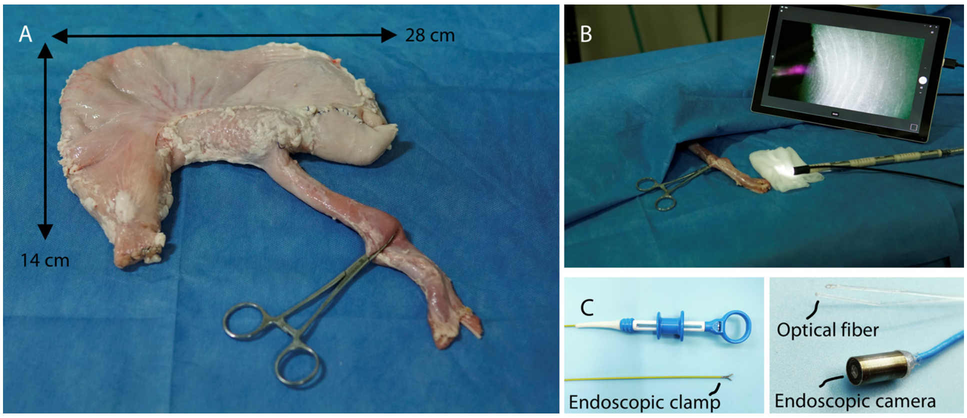

Fig. S10. Demonstration of therapy experiment in an excised porcine stomach. (**A**) The excised porcine stomach used in the therapy experiment was obtained from the Laboratory Animal Center of Zhejiang University with a length of 28 cm and a width of 14 cm. There was a tear in the fundus of the porcine stomach, which was sutured properly and left a small opening for an external camera. In addition, there was a small opening in the pylorus for the inflation tube. The pylorus was also closed by a suture preventing air leaks in the experiment. (**B**) The setup of elements in therapy experiment. (**C**) Endoscopic clamps from Micro-Tech (Nanjing) with a diameter of 2.0 mm. The diameter of the endoscopic camera is 4 mm.